Journal of Hydrology 529 (2015) 330–339

Contents lists available at ScienceDirect

Journal of Hydrology

journal homepage: www.elsevier.com/locate/jhydrol

Climate change and water storage variability over an arid endorheic region

Tao Yang [a,b,*], Chao Wang [a], Yaning Chen [b], Xi Chen [b], Zhongbo Yu [a,c]

[a] State Key Laboratory of Hydrology-Water Resources and Hydraulic Engineering, Hohai University, Nanjing 210098, China
[b] State Key Laboratory of Desert and Oasis Ecology, Xinjiang Institute of Ecology and Geography, Chinese Academy of Sciences, Urumqi, China
[c] Department of Geoscience, University of Nevada Las Vegas, Las Vegas, NV 89154-4010, USA

ARTICLE INFO

Article history:
Received 28 August 2013
Received in revised form 23 April 2015
Accepted 29 July 2015
Available online 4 August 2015
This manuscript was handled by Andras Bardossy, Editor-in-Chief, with the assistance of Axel Bronstert, Associate Editor

Keywords:
GRACE
GLDAS
Terrestrial water storage changes
Basin scale water balance

SUMMARY

Terrestrial Water Storage (TWS) plays an important role in regional climate and water resources management, especially in arid regions under global change context. However, serious lack of in-situ measurements in remote alpine mountains is hindering our current understanding of regional TWS change in the Tarim River Basin (TRB), a large and typical arid endorheic area in Northwest China of Central Asia. To solve the problem, four different hydrology products from the Gravity Recovery and Climate Experiment (GRACE) satellite, model simulations from Global Land Data Assimilation System (GLDAS) in conjunction with in-situ measurements, are utilized to investigate patterns and underlying causes of TWS and its component changes. An excess of precipitation over evapotranspiration (ET) plus runoff contributes to an increase of TWS. The phase of Total Soil Moisture (TSM) lags that of Snow Water Equivalent (SWE), indicating a recharge from snowmelt to TSM. Increasing TWS together with decreasing SWE resulted in an increase of subsurface water. Our results are of great value to amend basin-wide water management and conservation strategies for the similar arid regions considering climate change.

1. Introduction

Terrestrial Water Storage (TWS) plays a fundamental role within the global water, energy, and biogeochemical cycles (Famiglietti, 2004). TWS shapes climate and controls weather through a series of simple to complex processes and feedback mechanisms (Shukla and Mintz, 1982; Eltahir and Bras, 1996). However, TWS has not yet been measured with sufficient accuracy for vast areas due to lack of large scale monitoring means (Rodell and Famiglietti, 1999; Alsdorf et al., 2000; Lettenmaier and Famiglietti, 2006). The Gravity Recovery and Climate Experiment (GRACE) satellite mission was launched in March, 2002 with aims to observe large scale TWS variations (Tapley et al., 2004a). It has been demonstrated that seasonal and inter-annual changes in water storage for continental-scale patterns and for large river basins can be inferred from GRACE observations with an unprecedented accuracy (Tapley et al., 2004b; Ramillien et al., 2005; Schmidt et al., 2008). With the assistance of water storage components simulated by Global Land Data Assimilation System (GLDAS) (Rodell et al., 2004), GRACE can serve as a robust tool to estimate Groundwater Storage (GWS) variations at large basin or continental scales (e.g. Ramillien et al., 2008; Rodell et al., 2009; Shamsudduha et al., 2012).

The extremely arid Tarim River Basin (TRB) in northwest China experienced a steady rise in population since 1960, increasing the need for irrigation. The large scale irrigation in the TRB constitutes a major modification to the natural water balance (Li et al., 2009) and has triggered a range of environmental problems such as soil salinization (Brunner et al., 2007), the unproductive loss of water resources through phreatic evaporation (Brunner et al., 2008) and degradation of riparian ecosystems along the Tarim River (Schilling et al., 2014). Owing to increasing water consumption by modern oasis agricultural development, many rivers in TRB suffer a declining recharge from headstreams and tributaries and gradually lost their hydraulic connections with the main stream of Tarim River (Zhou et al., 2012). Climate and natural environment changes coupling with the regional continental climatic conditions will further deteriorate local water security.

Global warming and intensifying human activities have triggered precipitation and streamflow to change significantly in many regions around the world (e.g. Yang et al., 2008, 2010, 2014; Wang et al., 2014). There are a number of studies addressing the hydrometeorological processes via investigating the changing characteristics of precipitation, runoff and air temperature in the TRB

* Corresponding author at: State Key Laboratory of Hydrology-Water Resources and Hydraulic Engineering, Hohai University, Nanjing 210098, China. Tel.: +86 25 83786017.
E-mail address: yang.tao@ms.xjb.ac.cn (T. Yang).

http://dx.doi.org/10.1016/j.jhydrol.2015.07.051
0022-1694/

(e.g. Yang et al., 2011; Bothe et al., 2012; Zhou et al., 2012; Ling et al., 2013; Shang and Wang, 2013). Remote sensing together with Chloride Method have also been used to quantitatively evaluate the groundwater recharge rate and its distribution in analogous arid and semiarid regions (Brunner et al., 2004). However, so far no investigation concentrated on the vertically integrated TWS based on GRACE data over the TRB can be found. Due to the absence of in-situ equipment for precipitation, glacier, snowpack monitoring, especially in mountainous and desert regions (Fig. 1), little is known about large scale change patterns of hydrology cycle and water resources in TRB, thus seriously restricting to formulate sustainable water management strategies for arid region. Investigating the variability of water storage in the TRB is fundamental for a profound understanding of land-atmospheric and hydrological processes, and thus of great value for regional sustainable water resource management.

The objective of this work is to investigate the changing characteristics of TWS and its components and analyze the underlying causes of TWS variations in the TRB. A suite of GRACE hydrology products and simulations from GLDAS Land Surface Models (LSMs) are used to derive TWS states and fluxes. Results from different GRACE products and GLDAS simulations are quantitatively compared with each other as a cross-validation to evaluate the uncertainty, as compensation for the lack of in-situ measurements. Rainfall, snowfall, evapotranspiration (ET) and runoff (R) from GLDAS simulations as well as in-situ measured precipitation (P) are analyzed to identify the underlying causes of local TWS change. Our study will be of practical merit for a better understanding of the TRB's hydro-climatic variability to formulate sustainable water management strategies in similar arid endorheic regions.

2. Study region

TRB is China's largest endorheic basin with a drainage area of $1.04 \times 106\ km^2$ in Northwest China (Fig. 1). At an altitude of 800–8600 m, the basin slopes down from west to east, forming a typical sector-like pattern from its margin to its center, where is located the world famous Taklamakan Desert bordered by mountains and Gobi. The basin has four typical ring structures from the margin to the inside, with oasis and Gravel Gobi at the basin margin, desert at middle of the basin and Lop Nor at east of the basin.

The TRB has an extreme continental arid climate characterized by hot summers and cold winters, rare precipitation and strong evaporation. The mean annual temperature varies from 10.6 to 11.5 °C with 43.6 °C being the maximum and −27.5 °C being the minimum. The mean annual precipitation is 116.8 mm. Extremely uneven temporal and spatial distribution of water resources further results in a negative influence on highly efficient utilization of water resources. The variability and availability of water resources is a critical factor affecting the sustainability of regional socio-economy in the TRB, where agriculture development is heavily dependent on irrigation (Zhang et al., 2012).

Precipitation in TRB surrounding mountains plays an important role in recharging surface water and groundwater in downstream oasis and desert areas. Besides, seasonal melting water from mountain snowpack and glaciers also has a decisive effect on runoff processes (Yang, 1981). Located in the north part of TRB (Fig. 1), Tien Shan Mountain has shown significant regional climate change considering its temperature, precipitation, snowpack and glacier in global change context (Sorg et al., 2012). Almost all meteorological stations have recorded rising temperatures since the 1970s. Mean annual precipitation has increased in the outer (Aizen et al., 1997) and in the eastern ranges (Tao et al., 2011), but has decreased at higher altitudes in the inner ranges (Sorg et al., 2012). Increasing air temperatures have resulted in a decrease in the proportion of solid precipitation and enhanced snowmelt (Aizen et al., 1997; Qin et al., 2006). Glacier shrinkage in Tien Shan Mountain, especially in peripheral, lower-elevation ranges near the densely populated forelands, has led to significant seasonal alterations in runoff (Sorg et al., 2012). Precipitation, glaciers and snowpack change in

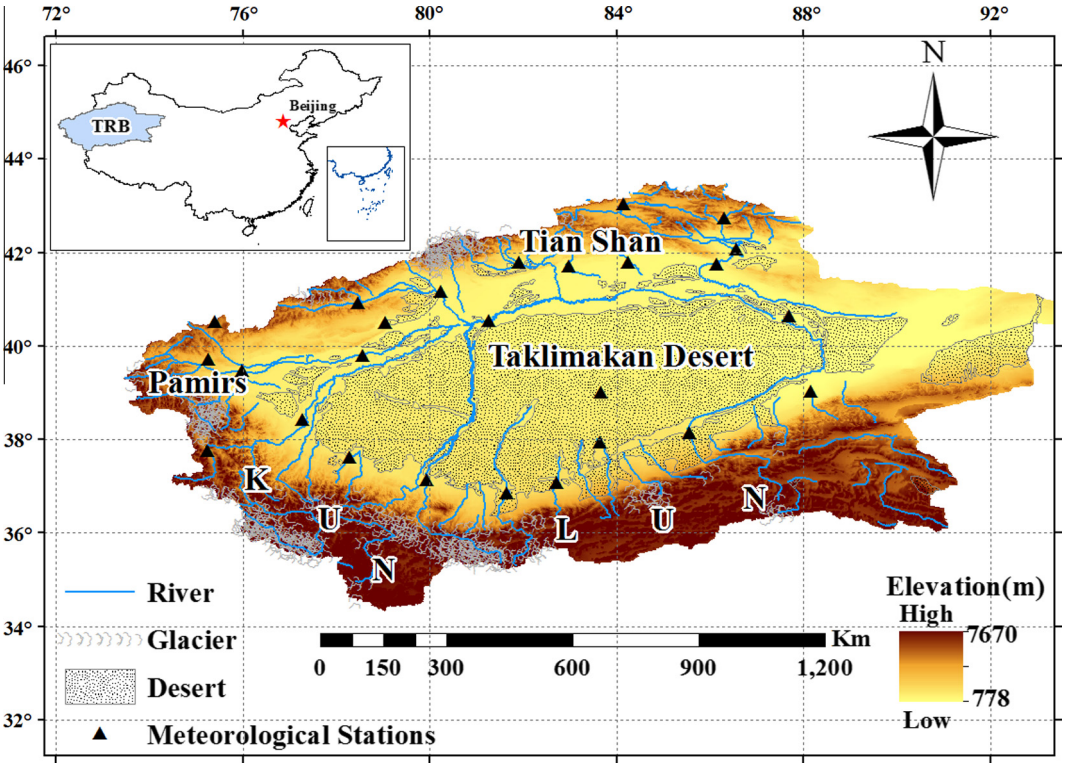

Fig. 1. Location of Tarim River Basin, a typical endorheic area in the Arid Region of Central Asia.

surrounding mountains of TRB have significant influences on regional runoff schemes.

3. Datasets and methods

3.1. TWS from an ensemble of GRACE products

The GRACE satellite project, jointly sponsored by NASA and the German Aerospace Center, has been collecting data since mid-2002. The nominal product of GRACE mission is a series of Earth gravity fields at ~30 intervals (Tapley et al., 2004b). By exploiting the direct relationship between gravity field changes and mass changes at the Earth's surface, the month-to-month Earth gravity field from GRACE is possible to detect vertically integrated TWS changes of 2–3 cm in Equivalent Water Height (EWH) over a basin greater than the GRACE spatial resolution of about 300 km (Swenson et al., 2003; Wahr et al., 2004).

In this study, four different gridded GRACE hydrology products published by the Centre for Space Research (CSR), the GeoForschungsZentrum (GFZ), the Jet Propulsion Laboratory (JPL) and Groupe de Recherche en Ge'odesie Spatiale (GRGS), were employed to derive TWS variations over the TRB.

The three gridded GRACE products provided by CSR, GFZ and JPL (hereafter referred to as CSR-, GFZ- and JPL-GRID respectively) are based on the latest Release-05 version gravity field coefficients (land grid version "scsv201209", available at ftp://podaac-ftp.jpl.nasa.gov/) (Swenson and Wahr, 2006). CSR, GFZ, and JPL all use different strategies to compute gravity field coefficients from the raw GRACE observations, while using similar background models for the ocean and the atmosphere (Chambers, 2006). Several tests have proven that RL05 dataset is more accurate and data from CSR, GFZ and JPL are more consistent with themselves than the previous RL04 data (Bettadpur, 2012; Chambers and Bonin, 2012). The model (Paulson et al., 2007) used to remove postglacial rebound signal in the RL05 data has been revised by Geruo et al. (2013). And the gaussian smoothing applied a radius of 200 km rather than 300 km as for land grid version "ss201008" (Swenson and Wahr, 2006; Landerer and Swenson, 2012). The scaling coefficients provided for each 1° bin of the GRACE gridded data are used to compensate bias and leakage and restore much of the energy removed by truncation, destriping and filtering processes (Swenson and Wahr, 2006).

The 10 day 1° × 1° GRGS GRACE time series data (version RL02; hereafter referred to as GRGS-GRID) provided by Centre National d'Études Spatiales (CNES) (Lemoine et al., 2007; Bruinsma et al., 2010) is available at http://grgs.omp.obs-mip.fr. This dataset is derived from GRACE GPS and K-band range rate data and from LAGEOS-1/2 satellite laser ranging (SLR) data (Bruinsma et al., 2010). These gravity fields are represented by a set of normalized spherical harmonic coefficients from degree 2 up to degree 50 using a stabilization approach without additional filtering. GRGS-GRID products do not require additional filtering, hence no scaling factor is applied for the GRGS-GRID data (Biancale et al., 2006; Ramillien et al., 2008; Tregoning et al., 2008). The 10 day GRGS-GRID solutions were converted to a monthly time series by taking the average values in order to directly compare them with other GRACE solutions employed here.

Missing GRACE data in CSR, GFZ, JPL (June 2003, January and June 2011) and GRGS (January, June 2003 and January 2011) time series were imputed (i.e., infilling of missing values) using linear interpolation and monthly mean values.

3.2. Global land data assimilation system

We apply monthly time series soil moisture estimates from four GLDAS simulations. GLDAS was developed corporately by the National Aeronautics and Space Administration Goddard Space Flight Center (NASA GSFC) and National Oceanic and Atmospheric Administration National Centers for Environmental Prediction (NOAA NCEP) (Rodell et al., 2004). GLDAS ingests satellite-, radar- and ground-based observational data products, using the state-of-the-art land surface modeling and data assimilation techniques, to generate optimal fields of land surface states (e.g., soil moisture, snow water equivalent and temperature) and fluxes (e.g., precipitation, ET and runoff). A number of studies using satellite-based hydrological fluxes and states observations and other hydrology model simulations have proved the applicability of GLDAS simulations in large scale water balance analysis (e.g. Rodell et al., 2007; Syed et al., 2008). Time series records of Total Soil Moisture (TSM) with a spatial resolution of 1° × 1° were derived from the four LSMs currently run in GLDAS, those are CLM (v. 2) (Dai et al., 2003), Mosaic (Koster and Suarez, 1992), Noah (Ek et al., 2003), and VIC (Liang et al., 2003). The total depth of soil column in CLM (10 layers), Mosaic (3 layers), Noah (4 layers), and VIC (3 layers) models are 3.4 m, 3.5 m, 2.0 m, and 1.9 m, respectively. However, neither GWS nor a surface water routing module was provided by these LSMs (Dai et al., 2003; Rodell et al., 2004).

Snowpack over surrounding mountains of TRB plays a fundamental role to local water supply as a huge solid water reservoir. Since the 1970s, almost all meteorological stations have recorded contrasting climate-driven precipitation changes and rising temperatures in these regions (Narama et al., 2010). In the second half of the twentieth century, decrease of both maximum snow cover thickness and snow cover duration have been observed at stations at all altitudes in Western and Central Tien Shan (Aizen et al., 1997). Climate-driven changes in mountain snow-melting fed streamflow regimes have direct implications on freshwater supply, irrigation dependent agriculture and hydropower potential. Hence, snowfields represented as (Snow Water Equivalent) SWE from GLDAS were used in our study to evaluate snow water storages changes in the TRB.

In addition, rainfall and snowfall from GLDAS forcings as well as ET and R from GLDAS simulations are also employed to evaluate GRACE Terrestrial Water Storage Change (TWSC) (defined as the difference in storage between any two successive periods) using surface water balance method.

GLDAS results are compiled in GRIB and NetCDF format and can be obtained from GES DISC at http://disc.sci.gsfc.nasa.gov/hydrology/data-holdings. Areal value of certain quantity is calculated from gridded data as weighted arithmetic mean, using the proportions of the area of a certain grid to the total area of the study region as weights.

3.3. In-situ measured precipitation

The precipitation data from 26 ground-based meteorological stations from January 2003 to December 2011 are used to validate GLDAS precipitation. The China Meteorological Data Sharing Service System of China Meteorological Administration (CMA) maintains stations across China with standard equipment for monitoring meteorological variables (http://cdc.cma.gov.cn/).

3.4. Data processing methods

Each GRCAE 1° × 1° monthly grid represents the gravity anomaly (GA below), that is, the difference between the gravity for that month (G) and the average gravity during a long term reference period (here is 01/2003–12/2011 in our study) ($\overline{G}$). This can be expressed as:

$$GA_j = G_j - \overline{G} \quad (1)$$

where the subscript j stands for the jth month. GRACE-observed gravity anomaly was then converted into Terrestrial Water Storage Anomaly (TWSA) using the relationship between gravity anomaly and TWSA (Swenson and Wahr, 2002). The four GRACE products used here are expressed as monthly gridded TWSA. Hence, each monthly grid represents the difference between TWS for that month (TWS_j) and the average TWS during 01/2003–12/2011 ($\overline{TWS}$). The relationship can be expressed as:

$$TWSA_j = TWS_j - \overline{TWS} \tag{2}$$

$$TWSA_{j+1} = TWS_{j+1} - \overline{TWS} \tag{3}$$

The difference of GRACE TWSA in two successive months can represent TWSC for a given basin at a monthly interval as follows:

$$TWSC_j = TWSA_{j+1} - TWSA_j \tag{4}$$

Based on water balance equation for a closed basin, $TWSC_j$ for a given basin can also be expressed as:

$$TWSC_j = \frac{P_{j+1}+P_j}{2} - \frac{ET_{j+1}+ET_j}{2} - \frac{R_{j+1}+R_j}{2} \tag{5}$$

Basin-scale average TWSA was estimated from scaled GRACE global fields as weighted arithmetic mean, using the proportions of the area of a certain grid included in the study region to the total area of the study region as weights. And the similar weighted arithmetic mean method was used to calculate basin-scale average results from original gridded products.

Point scale precipitation data at a certain time point from all stations are first interpolated into $1^\circ \times 1^\circ$ gridded data using inverse distance weighting method as:

$$u(\mathbf{x}) = \begin{cases} \frac{\sum_{i=1}^{N} w_i(\mathbf{x}) u_i}{\sum_{i=1}^{N} w_i(\mathbf{x})}, & \text{if } d(\mathbf{x},\mathbf{x}_i) \neq 0 \text{ for all } i \\ u_i, & \text{if } d(\mathbf{x},\mathbf{x}_i) = 0 \text{ for all } i \end{cases} \tag{6}$$

where $w_i(\mathbf{x}) = \frac{1}{d(\mathbf{x},\mathbf{x}_i)^p}$ is a simple inverse distance weighting function (Shepard, 1968). $\mathbf{x}$ denotes an interpolated (arbitrary) point, $\mathbf{x}_i$ is an interpolating (known) point, d is a given distance from the known $\mathbf{x}_i$ to the unknown point $\mathbf{x}$, N is the total number of known points used in the interpolation and p is a positive real number, called the power parameter. Areal precipitation was then calculated from gridded precipitation data as weighted arithmetic mean, using the proportions of the area of a certain grid included in the study region to the total area of the study region as weights.

Unweighted least square fitting is a basic signal processing approach in geophysics, especially in physical geodesy. The pattern of TWS variations is influenced by different kinds of geophysical processes. Seasonal cycles of the hydrological components were forced by the seasonal cycle of solar radiation, while inter-annual variability in the hydrological cycle was controlled by atmospheric circulation and precipitation (Eltahir and Yeh, 1999). So, TWS signal is a synthesis of signals with different periods. This approach was used to separate TWS signals of different periods and investigate the patterns and discuss the potential influences to signals of different periods.

The equation we used to fit TWS in this approach is:

$$TWS = A_{annual}\cos\left(\frac{2\pi}{T_{annual}}t + \varphi_{annual}\right) + A_{semi} \times \cos\left(\frac{2\pi}{T_{semi}}t + \varphi_{semi}\right) + bt + c, \tag{7}$$

where A_{annual} and A_{semi} are annual and semiannual amplitudes, T_{annual} and T_{semi} are periods of annual and semiannual cycles, and $T_{annual} = T_{semi} = 12$ months, b is the linear trend and c is a constant term.

4. Results and discussions

4.1. Comparison between GRACE and GLDAS over the TRB

The time series of GRACE-based TWSA (GRACE TWSA) and GLDAS simulated TSM plus SWE anomaly (GLDAS TWSA) spatially averaged over the TRB from January 2003 to December 2011 are shown in Fig. 2. Time series from the four GRACE products compare favorably with each other regarding their temporal evolutions, showing distinctive seasonal variations with water storage maxima generally found during the months of April to May and minima during October to November. TWS variations estimated from different GRACE products are strongly correlated with each other. The highest Pearson correlation ($r = 0.91$, p value < 0.0001) is observed between GRGS-GRID and CSR-GRID derived TWSA, and the correlation coefficients of TWSA signals derived from all different GRACE products can generally reach 0.70 with p value less than 0.0001.

The temporal variations of GLDAS-TWSA are coherent among the four GLDAS LSMs considering the phases of dry and wet periods (Fig. 2). The correlation coefficient between NOAH and VIC results is 0.94. This is perhaps not surprising since soil moisture changes are determined primarily by precipitation forcings that are the same for all models in GLDAS (Rodell et al., 2004). However, different amplitudes can also be found with NOAH showing the weakest annual amplitude while the MOSAIC showing the strongest (Fig. 2).

In the following analysis, we use the arithmetic mean of 4 GRACE-derived TWSA and 4 GLDAS-simulated (Total Soil Moisture Anomaly) TSMA and (Snow Water Equivalent Anomaly) SWEA. The standard deviation of water storage from different GRACE products and model simulations are employed to estimate the uncertainty of the final results.

4.2. Changes of TWSA storage components

Fig. 3 shows the temporal evolution of the mean GRACE TWSA, GLDAS TSMA and SWEA, and TWSA–TSMA–SWEA together with the standard deviation. TWSA, TSMA and SWEA exhibit significant seasonal variability. SWEA estimates, though limited in its geographic extent in mountain regions, contribute significantly to the averaged TWSA estimates by the virtue of the larger magnitude of snow water storage. On the other hand, TSMA estimates have a contrasting feature of a wider spatial extent but smaller magnitudes. Furthermore, peak TSMA storage lags that of SWEA, indicating the contribution of snowmelt to soil moisture recharge. SWEA exhibits a rapid increase during 2003–2005 while a decrease during 2005–2011 and thus results in an opposite trend in TWSA–TSMA–SWEA, i.e., a decrease during 2003–2005 and an increase during 2005–2011.

4.2.1. Intra-annual variability

The mean seasonal cycle of TWSA and its storage components is shown in Fig. 4. GLDAS SWEA peaks in April and reaches the lowest value in September with a seasonal amplitude of 45.1 ± 9.2 mm. Depending on the recharge of snowmelt from SWE, the phase of TSMA lags SWEA of 3–4 months. The relatively more abundant rainfall in July also contributes to more recharge thus higher magnitude to TSMA in July. The seasonal amplitude of TSMA is 17.7 ± 13.7 mm, about one third of that of SWEA. As an arid region featuring several different kinds of geomorphic types, the depth of unsaturated soil layer ranges from 3 m in riparian region to 50 m in desert and gobi region in the TRB (Dong and Deng, 2005). However, GLDAS models can simulate a depth of at most 3.5 m (Mosaic). Under-representation of TSM in areas with thick

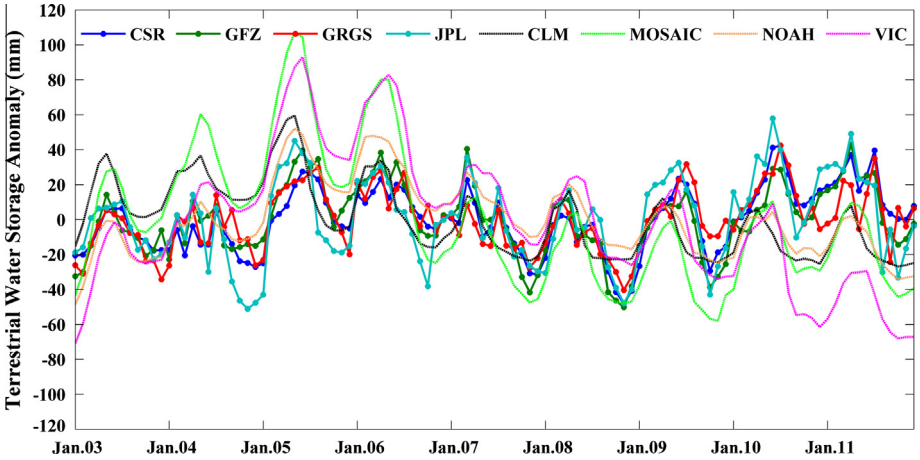

Fig. 2. Time series of TWSA from four different GRACE hydrology products and TSMA plus SWEA from four GLDAS LSMs.

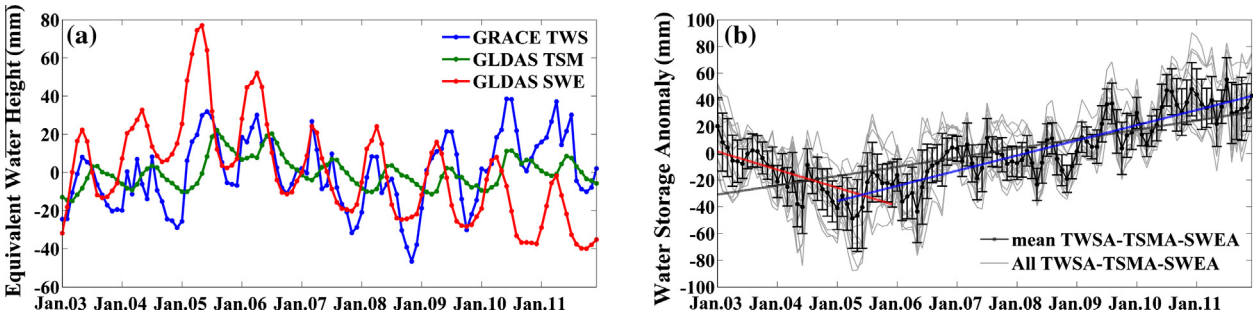

Fig. 3. (a) Monthly values of GRACE TWSA, GLDAS TSMA and GLDAS SWEA. (b) Monthly mean values of TWSA–TSMA–SWEA derived from all GRACE and GLDAS estimations, along with the error bars showing the uncertainty.

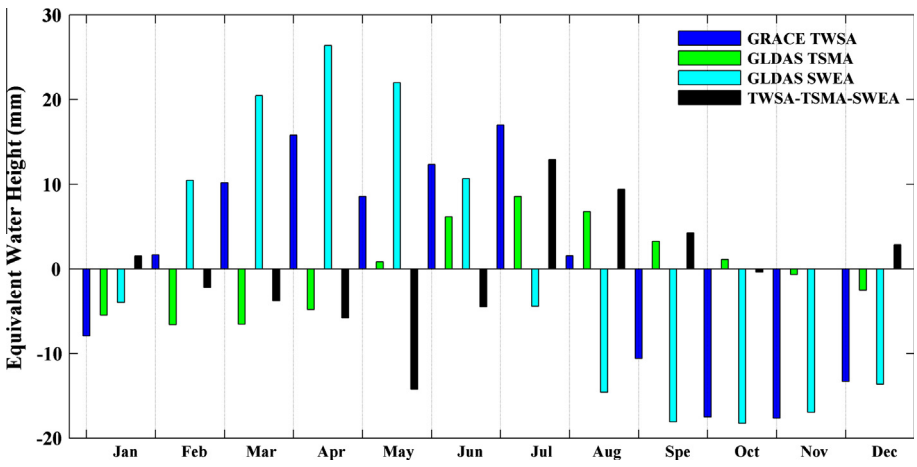

Fig. 4. Water storage seasonal cycle over the period 2003–2011 for GRACE TWSA, GLDAS TSMA and GLDAS SWEA. Together shown are GLDAS TSMA + SWEA and TWSA–TSMA–SWEA, an approximation of GWSA.

unsaturated zones can result in underestimation of the seasonal amplitude of TSMA.

GRACE TWSA peaks in April and July individually. The seasonal amplitude of GRACE TWSA is 39.6 ± 9.0 mm. The two peaks in GRACE TWSA can be attributed to peak value of SWE in April and that of rainfall in July respectively. As an enclosed endorheic basin, a large amount of surface and sub-surface water originates from melting water of snow cover and glacier.

Assuming there are little or no other factors resulting in the gravity change in this region except water storage variations, TWSA–TSMA–SWEA can be regarded as a valuable reference to investigate Groundwater Storage Anomaly (GWSA). As shown in Fig. 4, the seasonal amplitude of GWSA in the TRB is 31.6 ± 8.1 mm. GWSA increases during May to July and peaks in July due to abundant recharge from snowmelt and precipitation in summer.

4.2.2. Inter-annual variability

Inter-annual variability of GRACE TWSA and GLDAS TSMA + SWEA has been analyzed by subtracting annual, semiannual

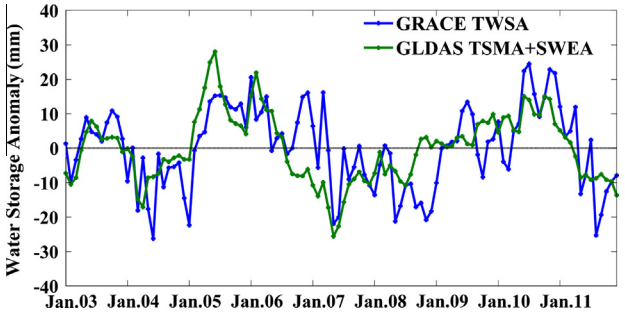

Fig. 5. Inter-annual variations of TWSA from GRACE and GLDAS after removing annual, semiannual and trend signals using an unweighted least square fit.

and trend signals calculated using an unweighted least square fit (Fig. 5). A good agreement with a correlation coefficient of 0.61 ($p < 0.0001$) is found between GRACE and GLDAS. The least square fitted annual and semiannual fluctuation of GRACE TWSA and GLDAS TSMA + SWEA matches well with each other in term of the amplitude and phase (not shown).

Improved correlation between GRACE and GLDAS after removing the seasonal and trend signals indicates that GLDAS can effectively simulate the inter-annual variability of TWS in spite of its exclusion of surface and groundwater terms. Thus inter-annual variability of TWS variation in the TRB region is mainly caused by TSM and SWE. And groundwater and surface water have no significant contribution to TWS inter-annual variability.

It is also revealed from Fig. 5 that the TRB region exhibits a nearly two year alternation of relatively dry and wet periods. It also corresponds well with the flood and drought condition as measured by yearly rainfall in Fig. 7(b), for instance, the continuous drought during 2007–2008 and the dramatic flooding in 2010.

4.2.3. Increasing GWS from increasing melting water

The changing rate of TWSA, TSMA, SWEA and GWSA in our study period are 1.6 ± 0.6 mm/year, 0.2 ± 1.0 mm/year, −5.5 ± 1.7 mm/year and 6.9 ± 2.2 mm/year (Fig. 3). Since GWSA is estimated by subtracting TSMA + SWEA from TWSA, the calculated increase in GWSA can be mainly attributed to the decrease of SWEA.

Snow and glaciers play an important role in stream flow regimes in arid regions with little summer precipitation. Maximum snow cover thickness has decreased by approximately 0.1 m and snow cover duration by 9 days between 1940 and 1991 in inner ranges of Tien Shan (Aizen et al., 1997). Analyses based on MODIS data for the period 2000–2007 confirm that the decrease in snow cover duration is persisting and that snowmelt now occurs earlier (Khalsa and Aizen, 2008). Intensified snow melt in regions surrounding the TRB may strongly affect the quantity

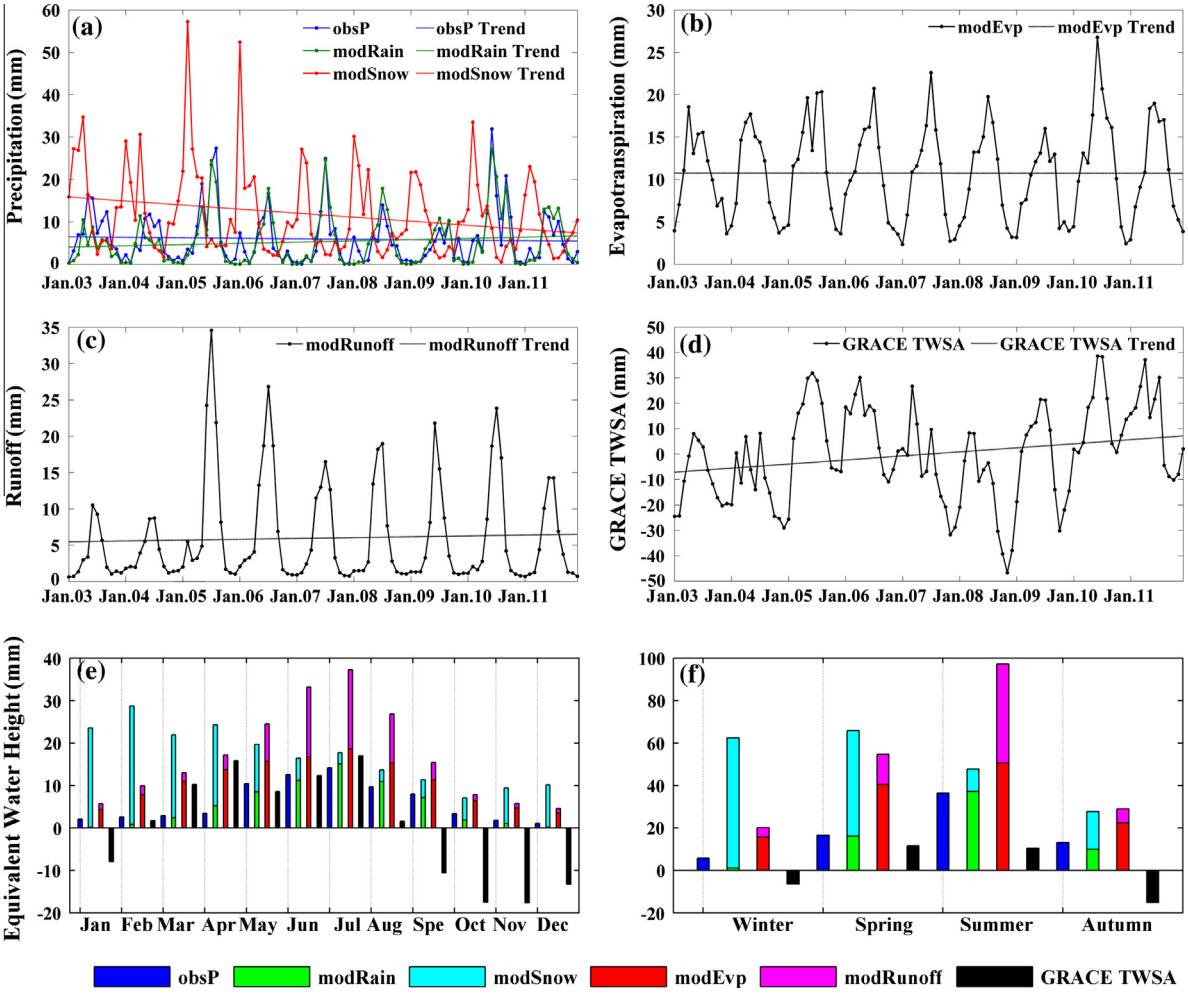

Fig. 6. Time series of monthly (a) observed precipitation, GLDAS-based rainfall, snowfall; (b) evapotranspiration, (c) runoff and (d) Gravity Recovery and Climate Experiment (GRACE) Terrestrial Water Storage Anomaly (TWSA), along with their average (e) monthly and (f) seasonal values for 2003–2011 in Tarim River Basin, the dashed lines show the linear trend.

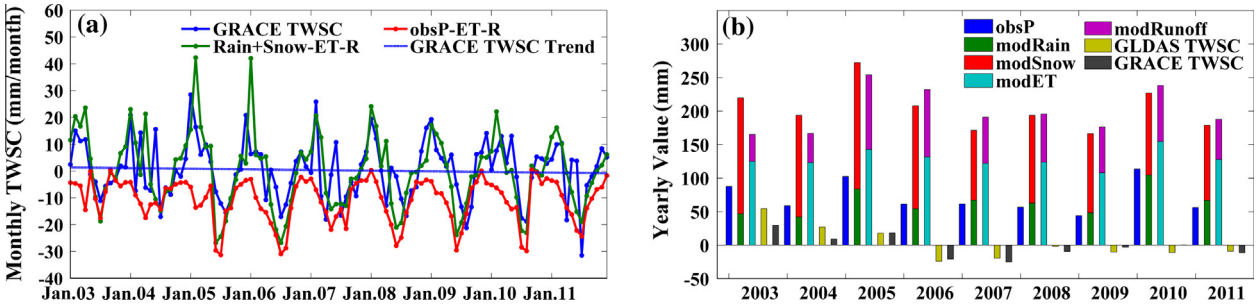

Fig. 7. (a) Comparison of Terrestrial Water Storage Change (TWSC) derived from Gravity Recovery and Climate Experiment (GRACE) with that derived from hydro-meteorological fluxes at monthly time scale; (b) yearly values of hydro-meteorological variables, GRCAE-derived and fluxes-derived TWSC.

and seasonal distribution of local runoff and increasing runoff has been observed in Tarim River in the past decades (Tao et al., 2011).

Increasing snow/ice melting water draining into the TRB may be the underlying cause of TWSA and GWSA increasing in our study. Lutz et al. (2014) project a consistent runoff increase in High Asia Mountains due to increasing glacier melt and precipitation. Since groundwater decrease have been observed in agriculture dominated mountain front regions (e.g. Li et al., 2009), our results indicate that melting snow and ice mainly recharge groundwater in inner-basin desert regions. Chen et al. (2012) analyzed the cause of the newly formed lakes in the Taklamakan Desert. Using the isotopic composition of water samples collected from the new lakes in the desert as tracers, together with data from remote sensing, local weather stations and stream gauges, Chen et al. (2012) inferred that the new lakes may originate from increased recharge of groundwater from meltwater in the nearby mountains. Here, our analysis based on GRACE and GLDAS results gives the similar inference as Chen et al. (2012) and further provides an estimate of GWS increasing trend.

However, shrinkage of ice and snow reserves may have a significant impact on the regional climate change and the sustainable development of water resources in the TRB. Intensified glacier melt in regions surrounding the TRB may strongly affect the quantity and seasonal distribution of local runoff. Our study calls attention to the formulation of new water management strategies considering water resources redistribution among different natural water reservoir. It also calls attention to the study of detection and utilization of groundwater resources in desert region (see Table 1).

Table 1
Definitions of abbreviations of hydrological quantities appeared in our study.

Abbreviations	Definitions	Unit
P	Precipitation	mm/month
ET	Evapotranspiration	mm/month
R	Runoff	mm/month
TWS	Terrestrial Water Storage	mm
TWSA	Terrestrial Water Storage Anomaly, defined as the time-variable residual water content relative to the long term mean water content during 2003–2011	mm
TWSC	Terrestrial Water Storage Change, the changing rate of TWS between two successive months	mm/month
SWE	Snow Water Equivalent	mm
SWEA	Snow Water Equivalent Anomaly	mm
TSM	Total Soil Moisture	mm
TSMA	Total Soil Moisture Anomaly	mm
GWS	Groundwater Storage	mm
GWSA	Groundwater Storage Anomaly	mm

4.3. Water balance and storage fluxes analysis

Fig. 6 shows time series of in-situ measured precipitation, GLDAS rainfall, snowfall, ET, R and GRACE TWSA at different time scales. The amplitudes are generally high in summer (June–August) and low in winter (December–January) except for GLDAS snowfall (see Fig. 6(a)–(f)). The fluctuations of the states/fluxes terms, as measured by the minima, maxima and mean values, along with the corresponding trends of the monthly, seasonal and annual time series are listed in Table 2.

GLDAS merges the strengths of both in-situ and space-borne observations and model simulations with the goal of maximizing spatial temporal coverage, consistency, resolution and accuracy (Rodell et al., 2004). The in-situ observed precipitation and GLDAS-based rainfall coincide well with each other considering the maxima, minima and mean values at different time scales (Table 2 and Fig. 6(a)). However, it should be noted that there were no snowfall records in the meteorological dataset from any CMA station in the study region during 2003–2011. This seems to be at variance with historical records (e.g. the snowfall event in the TRB in 2008) and can possibly be attributed to instrument failures, measurement drift or other problems. On the other hand, GLDAS snowfall mainly occurs in the South and North Slope of Kunlun Mountains (not shown). However, as shown in Fig. 1, there is no CMA station in the mountain regions and this could result in the absence of snowfall measurement.

TWSC derived from the GRACE observations and that derived from GLDAS storage fluxes of P, ET and R (hereafter referred to as flux-derived TWSC) are shown in Fig. 7. There are favorable agreements between the GRACE-derived and flux-derived TWSC (Fig. 7(a)). The correlation coefficient between GRACE TWSC and GLDAS P–ET–R is 0.66 with $p < 0.0001$. Fig. 8 illustrates the water balance considering the input (P), outputs (ET and R), GRACE TWSC (the difference of TWSA at the end and TWSA at the beginning of each time period) and GLDAS TWSC (P–ET–R) for each specific time period, with uncertainties estimated as standard deviation of different GRACE and GLDAS results. For 2003–2011, GRACE TWSC corresponds well with GLDAS TWSC. This indicates that water balance in the TRB can be closed successfully using GRACE TWSC and GLDAS P–ET–R, further indicates that GRACE and GLDAS results can be used in water balance analysis in our study region. However, GLDAS TWSC is larger than GRACE TWSC for 2003–2005 and smaller than GRACE TWSC for 2006–2008 and 2009–2011. The relative uncertainties of GLDAS TWSC are generally larger than that of GRACE TWSC and can mainly be attributed to the large uncertainties of R. Hence, though GLDAS has been proved to be robust in long term large scale terrestrial water balance analysis, the discrepancy among GLDAS LSMs should be reconciled in order to provide results with low uncertainty, especially in regional scale ungauged areas.

Also shown in Fig. 7(a) is the flux-derived storage change which employed the in-situ measured precipitation data instead of

Table 2
Statistical properties of the hydro-meteorological variables used in water storage analysis in Tarim River Basin.

Storage variable (mm)	Min	Max	Mean	Trend
Monthly value				
obsP	0.1	31.9	5.8	0
modRain	0.1	29.2	5.6	0
modSnow	0.5	57.2	11.6	−0.1
modP	2.4	59.4	17.0	−0.1
modET	2.3	26.8	10.7	0
modR	0.6	34.6	6.0	0
GRACE TWSA	−46.7	38.5	0	0.1
Seasonal value				
obsP	0.7	59.0	17.9	0
modRain	0.6	58.6	16.0	0.3
modSnow	6.4	86.7	34.8	−0.7
modP	21.0	95.4	50.9	−0.4
modET	11.1	64.7	32.2	0.1
modR	2.5	80.7	18.0	0.1
GRACE TWSA	−38.8	32.9	0	0.4
Yearly value				
obsP	44.1	113.7	71.5	−1.4
modRain	42.1	104.7	64.1	3.4
modSnow	104.3	188.5	139.4	−8.3
modP	166.3	272.2	203.5	−4.8
modET	107.9	154.6	128.8	0.5
modR	40.3	111.4	72.0	1.4
GRACE TWSA	−16.1	14.3	0	1.6

Abbreviations: obsP, in-situ observed precipitation; modRain, GLDAS-based rainfall; modSnow, GLDAS-based snowfall; modP, GLDAS-based precipitation, i.e. the summation of GLDAS rainfall and snowfall; modET, GLDAS-based evapotranspiration; modR, GLDAS-based runoff; and GRACE TWSA, GRACE derived terrestrial water storage anomaly.

GLDAS precipitation as the summation of rainfall and snowfall. The time series shows distinct discrepancy with GRACE-derived water storage, with negative water storage change occurs almost at all months. Negative water storage change at all months indicates a successive excess of ET + R over P, which would result in water storage decline in the study period. However, TWSA shows an increasing trend of 1.6 ± 0.6 mm/year during 2003–2011. Hence, though lack of in-situ measurements, it is of great necessity to involve snowfall from GLDAS in the equation in order to close the water budget in the TRB. The negative trend of TWSC could be attributed to the decrease of precipitation and the increase of ET and R (Table 2). Despite the negative TWSC trend, P is still larger than ET + R, hence the surplus P still added water to the study area and the TWSA exhibited an increase during the study period (Figs. 6(d) and 8(a), Table 2).

Table 3 shows the correlation between GRACE-derived TWSC and GLDAS-based hydrological variables. The correlations between modP and modET and modR were a little poor which is beyond our conventional expectation. However, as shown in Fig. 6(a) and (e), snowfall in winter accounts for a significant part in the GLDAS precipitation. With the spring coming, the increasing snowmelt water acts as a main source of ET and R. Hence, the correlations between modP and modET and modR can be obviously improved by employing a time lag of 3 months or 1 season in the time series (Table 3). Table 3 also indicates that GRACE TWSC correlates well with P, ET and R, suggesting that these storage fluxes are the main drivers of TWS change in the TRB.

4.4. Uncertainty analysis

Four different GRACE TWS products and four set of GLDAS LSMs outputs were used in our study. The reliability of GRACE and GLDAS to reveal large scale TWSC have been demonstrated in several regions where intense surface water, soil moisture and groundwater measurements exist. Syed et al. (2008) demonstrate that GLDAS can perform reasonably in capturing the global spatial patterns of observed storage changes at seasonal timescales. The study by Rodell et al. (2007) indicates that the GRACE–GLDAS estimates compared favorably with the well based time series for the Mississippi River basin and the two sub-basins that are larger than 900,000 km^2. Groundwater storage changes derived from GRACE TWS and GLDAS TSM correspond well to in situ borehole records in the Bengal Basin (Shamsudduha et al., 2012). Because of the lack of large scale in-situ soil moisture measurements, GLDAS-simulated soil moisture have been widely used in GRACE-related terrestrial water balance study (e.g. Ramillien et al., 2008; Rodell et al., 2009; Shamsudduha et al., 2012). All these studies demonstrated the applicability of GLDAS in large scale water balance analysis.

The correlation coefficients and standard deviation of different GRACE products and of different GLDAS results were further used to analyze the reliability of GRACE and GLDAS quantitatively. Though no in-situ measurements could be found to validate GRACE observations and GLDAS simulations, the coherence among different GLDAS products and different GLDAS outputs in our study region makes it more convincible that GRACE and GLDAS can be used here with a low uncertainty. The mean standard deviation

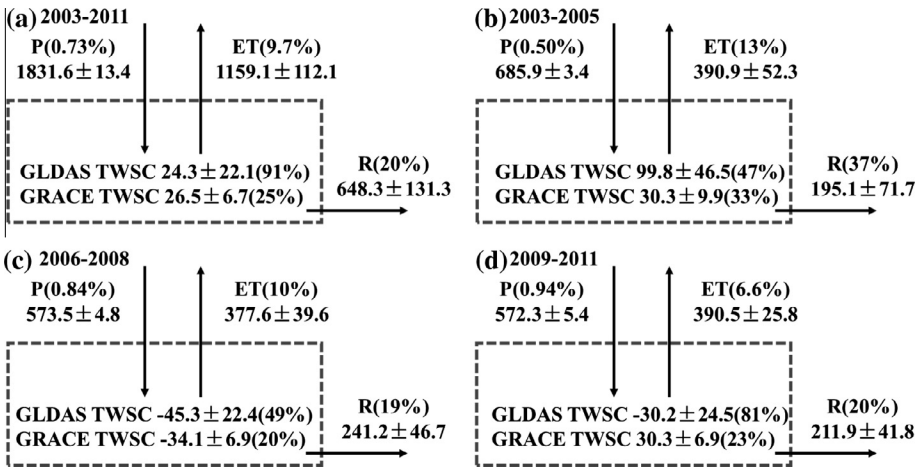

Fig. 8. Box scheme of water balance for different time periods. P, ET and R is the summation of each quantity during the specific time period. GLDAS TWSC is calculated as P–ET–R. GRACE TWSC is calculated as the difference between TWSA at the end and TWSA at the beginning of each time period. The uncertainties were estimated as standard deviation of different GRACE and GLDAS results and the relative uncertainties is shown in the parentheses (unit: mm).

Table 3
Correlation coefficients between GRACE-derived TWSC and GLDAS-based hydrological variables.

Correlation coefficients	modP	modE	modR	GRACE TWSC
Monthly value				
modP	1.00			
modET	0.35 (0.51)[a]	1.00		
modR	0.08 (0.47)	0.73	1.00	
GRACE TWSC	0.55	−0.52	−0.75	1.00
Seasonal value				
modP	1.00			
modET	0.27 [0.68][b]	1.00		
modR	0.06 [0.49]	0.78	1.00	
GRACE TWSC	0.42	−0.70	−0.80	1.00
Yearly value				
modP	1.00			
modET	0.75	1.00		
modR	0.54	0.52	1.00	
GRACE TWSC	0.40	−0.84	−0.85	1.00

[a] Values within parentheses are correlation coefficients with a lag of 3 month.
[b] Values within square brackets are correlation coefficients with a lag of 1 season.

is 7.2 mm among GRACE TWSA from different GRACE products, and 13.4 mm among GLDAS TSMA + SWEA from different LSMs, within the detectability of GRACE of ~1.0–1.5 cm equivalent water height (Wahr et al., 2004). According to previous studies and uncertainty analysis in our study, our results are reliable based on GRACE and GLDAS products.

5. Conclusions

The changing characteristics of TWS and its components and the driving factors are investigated based on GRACE hydrology products and GLDAS model simulations, together with in-situ measured precipitation data.

Considering the mean seasonal cycle of TWS and its components, GLDAS SWEA peaks in April and reaches the lowest value in September with an amplitude of 45.1 ± 9.2 mm. Depending on the recharge of snowmelt from SWE, the phase of TSMA lags SWEA of 3–4 months. The seasonal amplitude of TWSA–TSMA–SWEA in the TRB region is 31.6 ± 8.1 mm.

As to TWS inter-annual variability, a good agreement is found between GRACE TWSA and GLDAS TSMA + SWEA, indicating that GLDAS can effectively simulate the inter-annual variability of TWS in spite of its exclusion of surface and groundwater terms and inter-annual variability of TWS in the TRB region is mainly caused by TSM and SWE changes. In addition, TWS inter-annual variability corresponds well with the flood and drought condition as measured by yearly rainfall.

Increasing TWSA in conjunction with decreasing SWEA resulted in an increase of subsurface water. Melting water from decreasing SWEA are mainly from surrounding mountains and recharge GWS in inner-basin desert region. This inference corresponds well to previous study using isotopic method. And we further give an estimate of GWS increasing trend of 6.9 ± 2.2 mm/year. The increasing recharge to GWS from SWE melting leads to an increase in GWS and may contribute a lot to the relief of water crisis of water-depended agriculture.

Analysis of water balance indicates that water balance in the TRB can be closed successfully using GRACE TWSC and GLDAS P–ET–R and P decrease and ET + R increase result in a decrease of TWSC. However, an excess of P over ET + R still adds water to the TWS and contributes to an increase of TWSA time series. GRACE TWSC correlates well with P, ET and R, suggesting that these storage fluxes are the main drivers of TWS change in the TRB. No snowfall record can be found from in-situ observations. However, it is of great necessity to include GLDAS snowfall in order to close the water budget in the TRB. It further indicates that it is of great value to involve snowfall from multiple data sources, such as satellite observations, radar measurements, and reanalysis datasets, in order to compensate the inability of in-situ measurement systems to capture snowfall records while doing hydrologic research in such mountainous regions.

Acknowledgments

The work was supported by grants from the Chinese Academy of Sciences (KZZD-EW-12), National Natural Science Foundation of China (41371051), the Ministry of Science and Technology of China (2013BAC10B01), and a Grant from State Key Laboratory of Desert and Oasis Ecology (Y371163001). We thank JPL (NASA, USA) and GRGS (France) for GRACE products.

References

Aizen, V.B., Aizen, E.M., Melack, J.M., Dozier, J., 1997. Climatic and hydrologic changes in the Tien Shan, Central Asia. J. Clim. 10, 1393–1404.
Alsdorf, D.E., Melack, J.M., Dunne, T., Mertes, L.A.K., Hess, L.L., Smith, L.C., 2000. Interferometric radar measurements of water level changes on the Amazon flood plain. Nature 404, 174–177.
Bettadpur, S., 2012. UTCSR Level-2 Processing Standards Document for Level-2 Product Release 0005, GRACE 327-742, CSR Publ. GR-12-xx, Rev. 4.0, 16pp, University of Texas at Austin.
Biancale, R., Lemoine, J.-M., Balmino, G., Loyer, S., Bruisma, S., Perosanz, F., Marty, J.-C., Ge'gout, P., 2006. 3 Years of Geoid Variations from GRACE and LAGEOS Data at 10-day Intervals from July 2002 to March 2005, Report. Bureau Gravime'trique International, Toulouse, France.
Bothe, O., Fraedrich, K., Zhu, X.H., 2012. Precipitation climate of Central Asia and the large-scale atmospheric circulation. Theoret. Appl. Climatol. 108 (3–4), 345–354. http://dx.doi.org/10.1007/s00704-011-0537-2.
Bruinsma, S., Lemoine, J.-M., Biancale, R., 2010. CNES/GRGS 10-day gravity field models (release 2) and their evaluation. Adv. Space Res. 45 (4), 587–601. http://dx.doi.org/10.1016/j.asr.2009.10.012.
Brunner, P., Bauer, P., Eugster, M., Kinzelbach, W., 2004. Using remote sensing to regionalize local precipitation recharge rates obtained from the Chloride Method. J. Hydrol. 294 (4), 241–250. http://dx.doi.org/10.1016/j.jhydrol.2004.02.023.
Brunner, P., Li, H.T., Kinzelbach, W., Li, W.P., 2007. Generating soil electrical conductivity maps at regional level by integrating measurements on the ground and remote sensing data. Int. J. Remote Sens. 28 (15), 3341–3361.
Brunner, P., Li, H.T., Kinzelbach, W., Li, W.P., Dong, X.G., 2008. Extracting phreatic evaporation from remotely sensed maps of evapotranspiration. Water Resour. Res. 44 (8), W08428. http://dx.doi.org/10.1029/2007WR006063.
Chambers, D.P., 2006. Evaluation of new GRACE time-variable gravity data over the ocean. Geophys. Res. Lett. 33, L17603. http://dx.doi.org/10.1029/2006GL027296.
Chambers, D.P., Bonin, J.A., 2012. Evaluation of Release 05 time-variable gravity coefficients over the ocean. Ocean Sci. 8, 859–868.
Chen, J., Wang, C.-Y., Tan, H., Rao, W., Liu, X., Sun, X., 2012. New lakes in the Taklamakan Desert. Geophys. Res. Lett. 39, L22402. http://dx.doi.org/10.1029/2012GL053985.
Dai, Y. et al., 2003. The common land model (CLM). Bull. Am. Meteorol. Soc. 84 (8), 1013–1023.
Dong, X.G., Deng, M.J., 2005. Xinjiang Groundwater Resources. Xinjiang Science and Technology Press, Xinjiang.
Ek, M.B., Mitchell, K.E., Lin, Y., Rogers, E., Grunmann, P., Koren, V., Gayno, G., Tarpley, J.D., 2003. Implementation of Noah land surface model advances in the National Centers for Environmental Prediction operational mesoscale Eta model. J. Geophys. Res. 108 (D22), 8851. http://dx.doi.org/10.1029/2002JD003296.
Eltahir, E.A.B., Bras, R.L., 1996. Precipitation recycling. Rev. Geophys. 34 (3), 367–378.
Eltahir, E.A.B., Yeh, P.J.-F., 1999. On the asymmetric response of aquifer level to floods and droughts in Illinois. Water Resour. Res. 35 (4), 1199–1217.
Famiglietti, J.S. (2004). Remote sensing of terrestrial water storage, soil moisture and surface waters. In: Sparks, R.S.J., Hawkesworth, C.J. (Eds.), The State of The Planet: Frontiers and Challenges in Geophysics, Geophys. Monogr. Ser., vol. 150, pp. 197–207, AGU, Washington D.C. http://dx.doi.org/10.1029/150GM16.
Geruo, A., Wahr, J., Zhong, S.J., 2013. Computations of the viscoelastic response of a 3-D compressible Earth to surface loading: an application to Glacial Isostatic Adjustment in Antarctica and Canada. Geophys. J. Int. 192 (2), 557–572.
Khalsa, S.J.S., Aizen, V.B., 2008. Variability in Central Asia seasonal snow cover during the MODIS period of record. Geophys. Res. Abstr. 10, EGU2008-A-0443.
Koster, R.D., Suarez, M.J., 1992. Modeling the land surface boundary in climate models as a composite of independent vegetation stands. J. Geophys. Res. 97 (D3), 2697–2715. http://dx.doi.org/10.1029/91JD01696.

Landerer, F.W., Swenson, S.C., 2012. Accuracy of scaled GRACE terrestrial water storage estimates. Water Resour. Res. 48 (4), W04531. http://dx.doi.org/10.1029/2011WR011453.

Lemoine, J.-M., Bruisma, S., Loyer, S., Biancale, R., Marty, J.-C., Perosanz, F., Balmino, G., 2007. Temporal gravity field models inferred from GRACE data. Adv. Space Res. 39, 1620–1629. http://dx.doi.org/10.1016/j.asr.2007.03.062.

Lettenmaier, D.P., Famiglietti, J.S., 2006. Water from on high. Nature 444, 562–563.

Li, H.T., Brunner, P., Kinzelbach, W., Li, W.P., Dong, X.G., 2009. Calibration of a groundwater model using pattern information from remote sensing data. J. Hydrol. 377 (1), 120–130.

Liang, X., Xie, Z., Huang, M., 2003. A new parameterization for surface and groundwater interactions and its impact on water budgets with the variable infiltration capacity (VIC) land surface model. J. Geophys. Res. 108 (D16), 8613. http://dx.doi.org/10.1029/2002JD003090.

Ling, H.B., Xu, H.L., Fu, J.Y., 2013. High- and low-flow variations in annual runoff and their response to climate change in the headstreams of the Tarim River, Xinjiang, China. Hydrol. Process. 27 (7), 975–988. http://dx.doi.org/10.1002/hyp.9274.

Lutz, A.F., Immerzeel, W.W., Shrestha, A.B., Bierkens, M.F.P., 2014. Consistent increase in High Asia's runoff due to increasing glacier melt and precipitation. Nat. Clim. Change. http://dx.doi.org/10.1038/nclimate2237.

Narama, C., Kääb, A., Duishonakunov, M., Abdrakhmatov, K., 2010. Spatial variability of recent glacier area changes in the Tien Shan Mountains, Central Asia, using Corona (~1970), Landsat (~2000), and ALOS (~2007) satellite data. Global Planet. Change 71, 42–54.

Paulson, A., Zhong, S., Wahr, J., 2007. Inference of mantle viscosity from GRACE and relative sea level data. Geophys. J. Int. 171, 497–508. http://dx.doi.org/10.1111/j.1365-246X.2007.03556.x.

Qin, D., Liu, S., Li, P., 2006. Snow cover distribution, variability, and response to climate change in Western China. J. Clim. 19 (9), 1820–1833. http://dx.doi.org/10.1175/JCLI3694.1.

Ramillien, G., Frappart, F., Cazenave, A., Güntner, A., 2005. Time variation of land water storage from an inversion of 2 years of GRACE geoids. Earth Planet. Sci. Lett. 235, 283–301. http://dx.doi.org/10.1016/j.eps.2005.04.005.

Ramillien, G., Famiglietti, J.S., Wahr, J., 2008. Detection of continental hydrology and glaciology signals from GRACE: a review. Surv. Geophys. 29, 361–374.

Rodell, M., Famiglietti, J.S., 1999. Detectability of variations in continental water storage from satellite observations of the time dependent gravity field. Water Resour. Res. 35 (9), 2705–2723.

Rodell, M. et al., 2004. The global land data assimilation system. Bull. Am. Meteorol. Soc. 85 (3), 381–394.

Rodell, M., Chen, J., Kato, H., Famiglietti, J.S., Nigro, J., Wilson, C.R., 2007. Estimating groundwater storage changes in the Mississippi River basin (USA) using GRACE. Hydrogeol. J. 15 (1), 159–166. http://dx.doi.org/10.1007/s10040-006-0103-7.

Rodell, M., Velicogna, I., Famiglietti, J.S., 2009. Satellite-based estimates of groundwater depletion in India. Nature 460, 999–1003.

Schilling, O.S., Doherty, J., Kinzelbach, W., Wang, H., Yang, P.N., Brunner, P., 2014. Using tree ring data as a proxy for transpiration to reduce predictive uncertainty of a model simulating groundwater–surface water–vegetation interactions. J. Hydrol. 519 (B), 2258–2271. http://dx.doi.org/10.1016/j.jhydrol.2014.08.063.

Schmidt, R., Petrovic, S., Guntner, A., Barthelmes, F., Wunsch, J., Kusche, J., 2008. Periodic components of water storage changes from GRACE and global hydrology models. J. Geophys. Res. 113, B08419. http://dx.doi.org/10.1029/2007JB005363.

Shamsudduha, M., Taylor, R.G., Longuevergne, L., 2012. Monitoring groundwater storage changes in the highly seasonal humid tropics: validation of GRACE measurements in the Bengal Basin. Water Resour. Res. 48, W02508. http://dx.doi.org/10.1029/2011WR010993.

Shang, S., Wang, H., 2013. Assessment of impact of water diversion projects on ecological water uses in arid region. Water Sci. Eng. 6 (2), 119–130. http://dx.doi.org/10.3882/j.issn.1674-2370.2013.02.001.

Shepard, D., 1968. A two-dimensional interpolation function for irregularly-spaced data. In: Proceedings of the 1968 ACM National Conference, pp. 517–524. http://dx.doi.org/10.1145/800186.810616.

Shukla, J.Y., Mintz, 1982. Influence of land-surface evapotranspiration on the Earth's climate. Science 215, 1498–1501.

Sorg, A., Bolch, T., Stoffel, M., Solomina, O., Beniston, M., 2012. Climate change impacts on glaciers and runoff in Tien Shan (Central Asia). Nat. Clim. Change 2 (10), 725–731. http://dx.doi.org/10.1038/NCLIMATE1592.

Swenson, S., Wahr, J., 2002. Methods for inferring regional surface-mass anomalies from Gravity Recovery and Climate Experiment (GRACE) measurements of time-variable gravity. J. Geophys. Res. 107 (B9), 2193. http://dx.doi.org/10.1029/2001JB000576.

Swenson, S., Wahr, J., Milly, P.C.D., 2003. Estimated accuracies of regional water storage variations inferred from the Gravity Recovery and Climate Experiment (GRACE). Water Resour. Res. 39 (8), 1223. http://dx.doi.org/10.1029/2002WR001808.

Swenson, S., Wahr, J., 2006. Post-processing removal of correlated errors in GRACE data. Geophys. Res. Lett. 33, L08402. http://dx.doi.org/10.1029/2005GL025285.

Syed, T.H., Famiglietti, J.S., Rodell, M., Chen, J.L., Wilson, C.R., 2008. Analysis of terrestrial water storage changes from GRACE and GLDAS. Water Resour. Res. 44, W02433. http://dx.doi.org/10.1029/2006WR005779.

Tao, H., Gemmer, M., Bai, Y., Su, B., Mao, W., 2011. Trends of streamflow in the Tarim River Basin during the past 50 years: human impact or climate change? J. Hydrol. 400 (1–2), 1–9. http://dx.doi.org/10.1016/j.jhydrol.2011.01.016.

Tapley, B.D., Bettadpur, S.V., Watkins, M., Reigber, C., 2004a. The gravity recovery and climate experiment: mission overview and early results. Geophys. Res. Lett. 31, L09607. http://dx.doi.org/10.1029/2004GL019920.

Tapley, B.D., Bettadpur, S.V., Ries, J.C., Thompson, P.F., Watkins, M.M., 2004b. GRACE measurements of mass variability in the Earth system. Science 305, 503–505.

Tregoning, P., Ramillien, G., Lambeck, K., 2008. GRACE estimates of sea surface height anomalies in the Gulf of Carpentaria, Australia. Earth Planet Sci. Lett. 271, 241–244.

Wahr, J., Swenson, S., Zlotnicki, V., Velicogna, I., 2004. Time-variable gravity from GRACE: first results. Geophys. Res. Lett. 31, L11501. http://dx.doi.org/10.1029/2004GL019779.

Wang, X., Liu, H., Zhang, L., Zhang, R., 2014. Climate change trend and its effects on reference evapotranspiration at Linhe Station, Hetao Irrigation District. Water Sci. Eng. 7 (3), 250–266. http://dx.doi.org/10.3882/j.issn.1674-2370.2014.03.002.

Yang, L.P., 1981. Water Resources Distribution and Utilization in Xinjiang. Xinjiang People's Publishing House, Xinjiang.

Yang, T., Zhang, Q., Chen, Y., Tao, X., Xu, C., Chen, X., 2008. A spatial assessment of hydrologic alteration caused by dam construction in the middle and lower Yellow River, China. Hydrol. Process. 22 (18), 3829–3843. http://dx.doi.org/10.1002/hyp.6993.

Yang, T., Shao, Q., Hao, Z., Chen, X., Zhang, Z., Xu, C., Sun, L., 2010. Regional frequency analysis and spatio-temporal pattern characterization of rainfall extremes in the Pearl River Basin, China. J. Hydrol. 380 (3–4), 386–405. http://dx.doi.org/10.1016/j.jhydrol.2009.11.013.

Yang, T., Wang, X., Zhao, C., Chen, X., Yu, Z., Shao, Q., Xu, C.-Y., Xia, J., Wang, W., 2011. Changes of climate extremes in a typical arid zone: observations and multimodel ensemble projections. J. Geophys. Res. 116, D19106. http://dx.doi.org/10.1029/2010JD015192.

Yang, T., Wang, X., Yu, Z., Krysanova, V., Chen, X., Schwartz, F., Sudicky, E., 2014. Climate change and probabilistic scenario of streamflow extremes in an alpine region. J. Geophys. Res. 119 (14), 8535–8551. http://dx.doi.org/10.1002/2014JD021824.

Zhou, H.Y., Zhang, X.L., Xu, H.L., Ling, H.B., Yu, P.J., 2012. Influences of climate change and human activities on Tarim River runoffs in China over the past half century. Environ. Earth Sci. 67 (1), 231–241. http://dx.doi.org/10.1007/s12665-011-1502-1.

Zhang, Q., Singh, V.P., Li, J.F., Jiang, F.Q., Bai, Y.G., 2012. Spatio-temporal variations of precipitation extremes in Xinjiang, China. J. Hydrol. 434–435, 7–18. http://dx.doi.org/10.1016/j.jhydrol.2012.02.038.